Maximizing Friction by Passive Jamming

Halvor T. Tramsen,* Alexander E. Filippov, Stanislav N. Gorb,* and Lars Heepe

Many solutions for getting grip on varying substrates exist in nature and in technical applications, but they fail on substrate geometries they are not specifically designed for. A novel passive load-dependent system is developed that creates high friction forces on a large variety of substrates: the granular media friction pad. With an elastic membrane encasing granular media, it reversibly undergoes the jamming transition only by varying the normal load. Here, the friction performance on different substrates is shown and the underlying physical mechanisms in a numerical simulation are investigated.

Locomotion often relies on a stable attachment that requires the ability of getting grip by creating high adhesion and friction forces between two surfaces in contact. In biology, two different ways of tackling this challenge are observed: specialized systems for a specific, predictable substrate on the one hand, and generalist systems combining different approaches to cope with a broad variety of substrates, e.g., wet or dry, soft or hard, smooth or rough, on the other.[1] Specialized systems include the head-arresting system of dragonflies,[2,3] wing locking mechanisms in beetles,[4] or parasitic louse flies holding onto feathers.[5] These systems feature specifically shaped, highly effective structures, optimized to work with one corresponding substrate but failing in contact with other surfaces. Generalist systems however achieve grip on a diversity of substrates, using a combination of mechanisms each optimized for different substrate types. Typical examples include insects that, during hunt for food, need stable grip on all surfaces to follow their prey. Their feet[2,6–8] use claws for mechanical interlocking on rough substrates, elongated hair-like structures for attaching to small surface asperities, and spatulae for adhesion on smooth substrates. Another example for the generalist system is the locomotion of snakes, who rely on a combination of muscle-induced local change of stiffness,[9] the anisotropy of their scales[9,10] and the scales' anisotropically microstructured surfaces.[11,12]

H. T. Tramsen, Prof. A. E. Filippov, Prof. S. N. Gorb, Dr. L. Heepe
Department of Functional Morphology and Biomechanics
Zoological Institute
Kiel University
D-24118 Kiel, Germany
E-mail: htramsen@zoologie.uni-kiel.de; sgorb@zoologie.uni-kiel.de
Prof. A. E. Filippov
Donetsk Institute for Physics and Engineering
National Academy of Sciences of Ukraine
83114 Donetsk, Ukraine

The ORCID identification number(s) for the author(s) of this article can be found under https://doi.org/10.1002/admi.201901930.
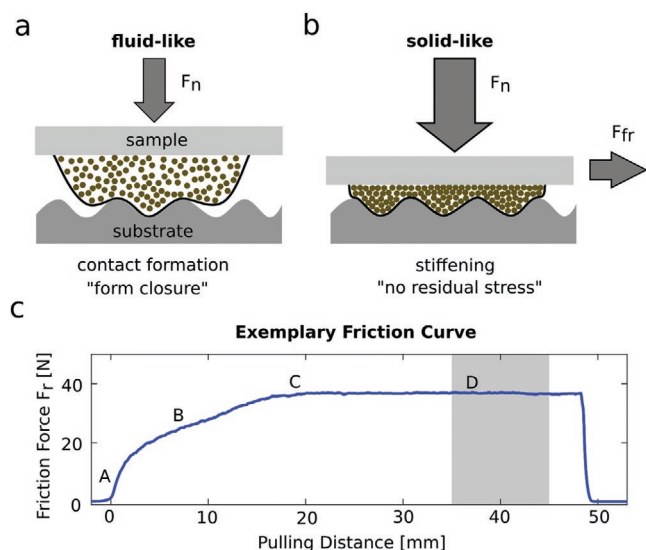
Technological applications of adhesion and friction mechanisms mostly specialize on one specific substrate, e.g., hook-and-loop fasteners, or car tires optimized for different environments and conditions, such as high performance tires, road tires or mud tires, tires for different temperatures in summer or winter, for wet or for dry roads. Similarly, robotic systems with optimized foot structures, such as gecko-like structures for climbing flat surfaces[13,14] or micro spines for climbing rough terrain,[15,16] decrease rapidly in performance and predictability when used in less ideal environments.

How would an engineered solution using the generalist approach need to be designed in order to maximize friction forces on all substrates, which could be flat, rough, structured or arbitrarily shaped, clean or contaminated?

In this letter we introduce a novel passive load-dependent jamming system that is able to create high friction forces on a variety of different substrates: the granular media friction pad (GMFP). It consists of a thin elastic membrane encasing a granular material that reversibly undergoes the jamming transition only by varying the normal load of the system. When coming into contact with any kind of substrate, the flexible membrane conforms to the substrate and creates a large real contact area.[17] The granular material encased by the membrane is loosely packed and behaves like a fluid,[18,19] enabling it to conform to the substrate, which results in a minimum of stored elastic deformation energy at the interface to maximize adhesion-mediated friction[20,21] (see **Figure 1**a). Upon applying normal load, the granular material undergoes the jamming transition[22,23] and becomes solid-like (see Figure 1b). This results in high friction forces generated by both the granular material as well as the membrane. The rigidified granular material generates these forces by mechanical interlocking and presumably by energy dissipation due to high friction between the densely packed particles.[24–29] The membrane generates friction forces by the strong deformation of the thin elastic membrane but also by adhesive interaction with the substrate.[30,31] Once the normal load is removed, the granular material returns to a fluid-like state, and so the sample can be removed easily from the substrate without requiring high pull-off forces.

To study this novel friction-enhancing system, we investigate the jamming transition of the GMFP. We then characterize its friction coefficient on different clean and contaminated substrates and examine the interplay of the different physical mechanisms by developing a numerical model. To assess the GMFP's performance, we will compare it to two other types of samples made from bulk silicone (see **Figure 2**a): a spherical shape resembling the form of an unloaded GMFP, and a 3 mm high flat cylinder with the same base area as the GMFP. Details regarding the samples employed, the experimental setup as

**ADVANCED
SCIENCE NEWS**
www.advancedsciencenews.com

**ADVANCED
MATERIALS
INTERFACES**
www.advmatinterfaces.de

Figure 1. Schematic drawing of the granular media friction pad (GMFP): a soft membrane encasing granular material. a) Fluid-like behavior when approaching the substrate, b) solid-like behavior under normal load F_n resulting in high friction forces F_{fr}. c) Exemplary friction curve showing the phases of the pulling curve at $F_n = 19.36$ N: A) shearing of granular material, B) shearing of granular material and elastic deformation of membrane, C) static friction peak, and D) dynamic friction.

well as the numerical model are discussed in the experimental section at the end of this article.

An exemplary friction curve of a GMFP on a clean flat substrate at a normal load $F_n = 19.36$ N is shown in Figure 1c. The friction behavior consists of four regimes: A) First, only the jammed granular particles are sheared, leading to a steep incline. B) In addition to the shearing of the particles, the flexible membrane is being stretched, leading to a low incline in friction force F_r. C) Marks the point of the transition from static friction to global dynamic friction (D). Upon removing shear and normal load from the system, the membrane's strain causes the GMFP to mostly relax to its initial configuration. To obtain the dynamic friction forces, 10s of the sliding force were averaged (gray area in Figure 1c).

To demonstrate the GMFP's jamming behavior, the stiffness of the samples was obtained from the slope of the force–displacement curves for different normal loads (see Figure 2b). In the first few seconds of the experiment, the force curve of the GMFP exhibits a distinct initial linear slope before flattening. Here, the forces resulting from the small deformation of the membrane are considered to be negligible[32] in comparison to the forces generated by the granular material (see Video S1 in the Supporting Information). This linear part, which is of different duration depending on the normal load, is fitted and the resulting slope is shown in Figure 2c, clearly showing the GMFP's jamming transition.[22,33,34] The increase in normal load in combination with the deformation of the encasing membrane is sufficient for the particles to undergo the jamming transition without needing outside forces, e.g., vacuum[18,35] or surrounding solid walls.[23] For low normal loads F_n, the GMFP is the softest of the three samples, while at high F_n, the GMFP's stiffness is comparable to the flat bulk silicone sample. The spherical sample is rather soft under all normal loads since its
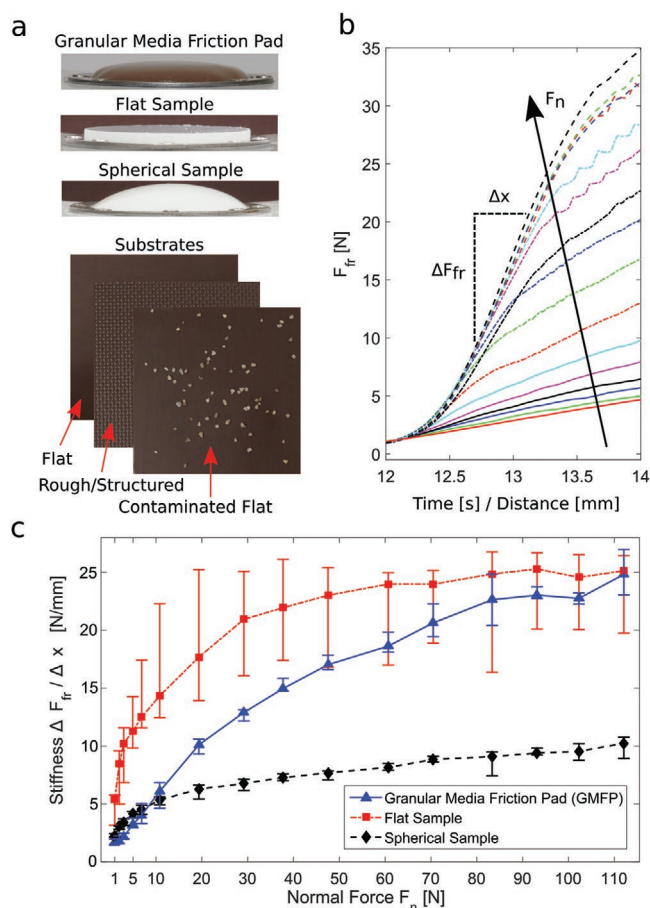

Figure 2. a) Photographs of the three samples (40 mm diameter) and the three substrates (100 mm × 100 mm). b) Slope of the force curve F_{fr} at the beginning of the experiment. Normal load F_n ranges from the sample weight (1 N) up to the maximum load of 112.09 N. c) Initial stiffness of the samples showing the jamming transition of the GMFP from very soft to stiff, the data points showing the median, the error bars showing the minimum and maximum values.

elongated shape facilitates bending more than the flat sample of the same material. For the flat sample, a high stiffness even at low load was expected. The opposite was observed since initial strain due to fixation of the sample resulted in small and unstable contact areas at low normal loads. The spherical sample and the GMFP did not exhibit this behavior, since they are much less prone to strain by design.

The results of the friction experiments on all substrates are shown in **Figure 3**a–c. At $F_n = 19.36$ N, resulting friction forces on the clean flat substrate exceed $F_r > 35$ N (see left column of Figure 3a) and are of the same order as forces that universal grippers using granular jamming in combination with active vacuum switching can achieve (see, e.g., Supporting Information for [18], where a gripper bag with a radius 4.3 cm is pulled over a test sphere achieving maximum friction forces of $F_r \approx 34$ N with a similar contact area as the GMFP).

On the flat substrate (see Figure 3a), the GMFP exhibits extremely high friction forces at low normal load. This can be attributed to the high adhesion forces of the GMFP's flexible membrane.[20,36] While the flat silicone sample would be expected to perform equally well, the minimal stress caused by
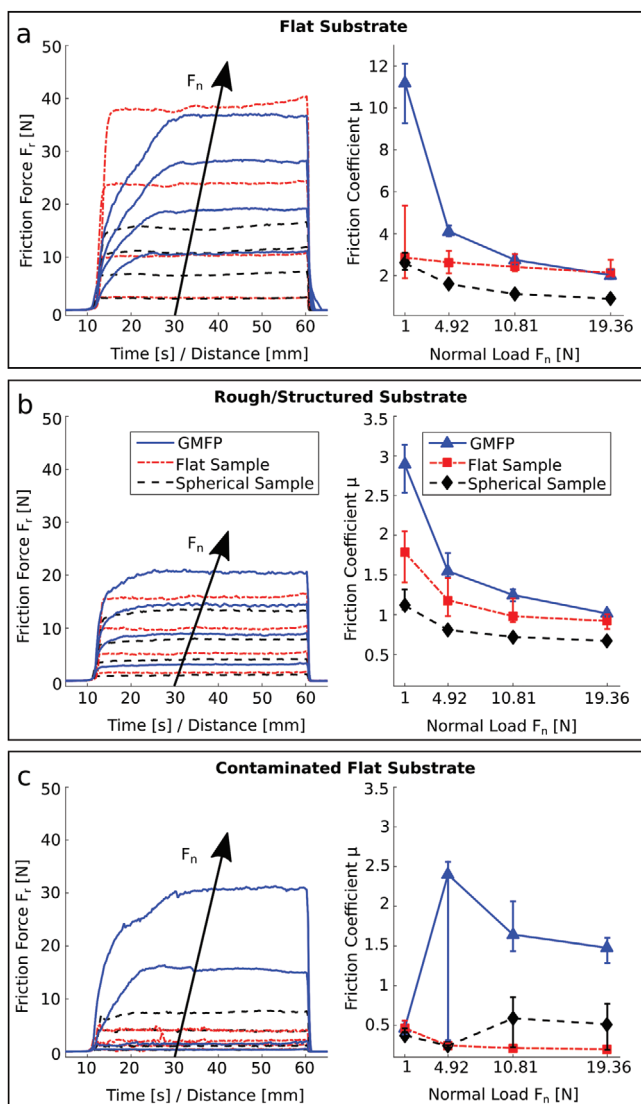
Figure 3. Friction performance (left column) and resulting friction coefficients (right column) of all samples on a) the flat substrate, b) the rough/structured substrate, and c) the contaminated flat substrate.

the fixation of the sample onto the sample holder leads to a slight deformation of the flat silicone. The sample's own weight cannot sufficiently flatten the sample to create a larger contact area for adhesion-mediated friction. The spherical sample cannot achieve large contact areas under any loading conditions, thus achieving lower friction forces than the other two samples for all normal loads. The GMFP shows a much later onset of sliding friction compared to the bulk silicone samples. Also it deforms strongly before sliding begins (see Video S2 in the Supporting Information), while still being able to create large contact areas during sliding (see Video S3 in the Supporting Information).

On the structured substrate (see Figure 3b), friction forces are generally lower since contact area between sample and substrate is reduced due to surface corrugations and higher roughness of the substrate. Nevertheless, the GMFP achieves highest friction coefficients for all normal loads due to its adaptability at contact formation and deformability during sliding.[37,38]

On the flat substrate contaminated by large particles (see Figure 3c), the flat and spherical samples exhibit very low friction, which is mostly dominated by third body friction due to the rolling gravel between sample and substrate. The GMFP's performance is entirely different, greatly exceeding that of the bulk silicone samples (see Video S4 for a side view and Video S5 for a visualization of the contact area in the Supporting Information). At low normal forces, the elastic membrane's tension is so high that it only lies atop the contaminating particles without yet reaching the substrate. At higher normal loads, the granular media push the membrane around the particles, creating large contact areas and a high friction coefficient. In comparison to the rubber bulk samples, the thin elastic membrane requires much less force to squeeze around the particles and to get in contact with the substrate even at lower normal forces.[17] This high adaptability resulting from the membrane as well as the granular material[35] enables the GMFP to achieve high friction forces although the contaminating particles are half the size of the GMFP's height.

In addition to the experiments, we newly developed a numerical 2D model (see the Experimental Section). This minimalistic but realistic model is used to describe how the occurring friction forces are composed of forces stemming from the granular material as well as from the elastic membrane. This can be seen in **Figure 4**, where the total friction force (Figure 4a) results from the addition of the forces generated by the membrane (Figure 4b) and of the forces generated in the granular material (Figure 4c). As can be seen, at the beginning of the experiment, friction forces generated by the granular media clearly dominate the friction properties of the GMFP. Only after a longer sliding distance, friction forces from the deformation of the membrane contribute to the total friction force, thus clearly showing the relevance of the rigidified granular material to the total friction properties of the GMFP. The range of normal load shown here ranges from the GMFP just touching the substrate to the highest compression numerically and physically reasonable, where the effect of rigidification of the granular material is clearly visible from the strong increase of the slope at the beginning of the force curve in Figure 4c similar to the change in slope of the force curve seen in Figure 2b.

To visualize the contact dynamics of the GMFP when sliding on a substrate, the motion of the sample when sliding is plotted in Figure 4d. Here, the green outer area displays the motion of the GMFP over time. Static contact of the elastic membrane on the substrate is displayed in yellow, dynamic sliding contact in blue. We distinguish between static and dynamic by time-dependent adhesion. When the membrane stays longer in contact with the substrate, the color transitions from blue to yellow, thus indicating a long static contact. When sliding starts at $t = 0$, only the outer regions of the GMFP in contact move on the substrate. This can also be seen in the Videos S2–S5 in the Supporting Information of the physical sliding experiments, where the sample deforms while the contact area remains static. This can also be seen in the simulation in Figure 4d. The contact area stays on the same position while the overall sample moves sideways. Due to the deformation of the membrane, the static contact area grows smaller at the forefront of the sliding until eventually global sliding sets in (yellow area completely
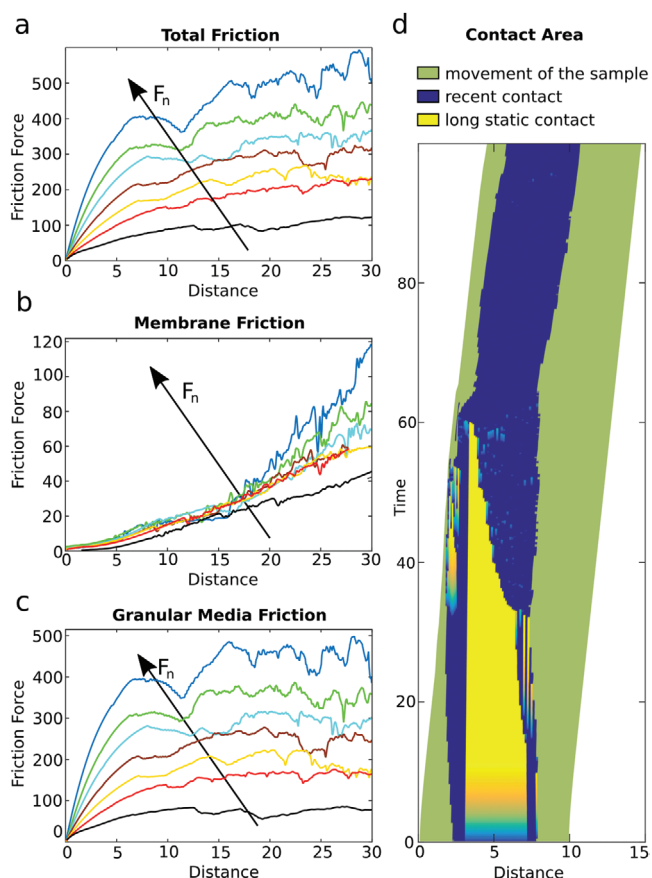
Figure 4. Numerical simulation of the granular friction pad. a–c) Friction forces in dependence of normal load F_n: a) Total friction force of the sample, b) friction force generated by membrane deformation, and c) friction force generated by the granular media. d) Visualization of the GMFP's contact area: The outer green area represents movement of the whole sample, the dark blue center area represents the contact area between sample and substrate, and the center transition from blue to yellow shows time-dependent adhesion of the membrane in contact with the substrate.

vanishes). In contrast to bulk materials such as the investigated flat and spherical samples, the GMFP can remain in static contact for a very long time. Where other samples would already start with dynamic sliding, the GMFP still remains in static contact. While Figure 4d is plotted for the second lowest normal force plotted in Figure 4a–c, this behavior could be seen for all normal forces. By using particle image velocimetry,[39,40] the same behavior could also be shown in the physical sample (see Video S6 in the Supporting Information).

To summarize, we introduced a GMFP, consisting of granular media encased by an elastic membrane, that shows high friction forces on a large variety of substrates. Under low normal load, it behaves as a fluid-like material which can greatly adapt to the substrate geometry, thus creating large contact areas. Under high normal load, the GMFP undergoes the jamming transition and becomes solid-like. Here, the energy dissipation by interparticle friction and membrane deformation leads to high friction forces during pulling along all substrates and under varying normal loads. Even on substrates covered by 1–2 mm particles, the GMFP is able

to create large contact areas and shows a robust design against stick and slip, since strong deformation has to occur before global slipping starts. A numerical simulation confirmed these experimental findings and clearly showed the interplay between granular material and membrane for creating friction.

For future research, a detailed study will investigate the effect of changing the GMFP's adaptability to substrates by altering the membrane as well as by increasing interparticle friction of the granular media.[41] In this work we decided to focus on dry substrates, however a detailed analysis using a structured membrane well known for its high friction performance on wet substrates will be conducted.[42]

Being able to create high friction on diverse substrates, the GMFP is suited for a variety of use cases where stable grip on substrates is important. The GMFP is passive and requires no control at all, it features easy lift off the substrate after unloading since no pressure difference has to be eliminated[43] and shows high damping properties.[35,44] Therefore, one possible application is the use as a foot for robotic applications. This system is especially suited for heavy walking robots[45,46] since a higher robot weight leads to a stiffer GMFP with increased friction due to particle jamming.

Experimental Section

Granular Media Friction Pad: The GMFP consisted of a 0.45 mm thick circular silicone membrane (40 mm diameter) that was fixed at the edge on a flat sample holder and filled with 1.7 g of ground coffee. The silicone material used to cast the membrane was Dragon Skin™ 30 (Smooth-On, Inc., PA, USA) with a Young's Modulus of (0.53 ± 0.02) MPa. For the granular media, ground coffee was chosen (Gold 100% Arabica, Markus Kaffee GmbH & Co. KG, Weyhe, Germany). The particle size data were obtained by sieving 3 batches of 25 g of ground coffee and is given in **Table 1**. When the GMFP was filled with 1.7 g ground coffee, the volume fraction was (51 ± 2)%.

In addition, two other types of samples were cast from bulk silicone also made from Dragon Skin™ 30 (see Figure 2a): A sample with a spherical shape to represent the GMFP in the unloaded state as well as a flat cylinder with 3 mm height and the same base area as the GMFP. All sample types were produced four times and each sample was tested on three different substrate types in random order.

The substrates were chosen to represent a wide variety of surfaces: a flat substrate (the flat side of wire mesh plywood), a rough/structured substrate (the structured side of wire mesh plywood), and a flat substrate contaminated by particles (the flat side of wire mesh plywood contaminated by 0.5 g of 1–2 mm gravel particles) (see Figure 2a).

Substrate and sample could freely move on low-friction linear bearings that were free of play. The substrate was pulled horizontally at

Table 1. Granular media (ground coffee) particle sizes.

Sieve size [µm]	Mass [%]
<125	0 ± 0
125	1.5 ± 2
250	46.6 ± 3
500	50.5 ± 4
1000	1.4 ± 1
2000	0 ± 0

1 mm s^{-1} for 50 mm using a linear testing machine (Xforce HP 500N, ZwickiLine, Zwick Roell, Ulm, Germany) that measured the pulling force. The sample could move vertically above the substrate while the substrate was slid sideways underneath. Additional weights could be placed on the sample to increase normal load during the experiment. The friction generated by the experimental setup itself did not exceed 0.2 N under all loading conditions and due to the much higher friction forces caused by the GMFP and the other samples, this is considered negligible for the discussion of the results. To achieve precise and reliable results, the sampleholder needs to be sufficiently mobile while being lightweight to examine a mostly uncompressed GMFP (total weight including bearings 1 N) but also sufficiently strong to withstand high friction forces at high normal loads. Thus, a small torsion at higher loads can be observed (see Video S4 in the Supporting Information) but is very small compared to the total deformation of the GMFP.

Numerical Simulation: For the numerical simulation, the granular particles ($N = 200$) were modeled by a Gaussian repulsion with effective interaction radius r_{02}. The elastic membrane was modeled by single points ($N = 200$) connected by springs with anisotropic elastic constants. The membrane connected to the sample holder at both ends and membrane and particle properties were adjusted to obtain the best coincidence between equilibrium shape of the membrane and its form in the physical experiment. After an initiation period, the modeled GMFP was pulled over a flat substrate at a constant normal load (see the Supporting Information for an illustration of the model and the initiation period). Friction was modeled by energy dissipation due to velocity v_j dependent forces $F = \eta_i (v_1 - v_2)$ with tunable friction η_i for particle–particle, particle–membrane, and particle–sampleholder interaction. Friction forces at the contact area between membrane and substrate were modeled as dry friction, where motion was initiated after a critical force threshold F_{eff} was exceeded. This force threshold consists of a material-dependent constant F_0 and an adhesion-dependent component increasing with contact time τ_j, resulting in an effective threshold force of $F_{eff} = F_0[1 + B_1 \tau_j/(1 + B_2 \tau_j)]$, which is proportional to the time τ_j at short timescale and saturates after a while, with the time defining constants B_1 and B_2.

Supporting Information

Supporting Information is available from the Wiley Online Library or from the author.

Conflict of Interest

The authors declare no conflict of interest.

[1] S. N. Gorb, *Philos. Trans. R. Soc. A* **2008**, *366*, 1557.
[2] S. N. Gorb, *Biological Micro- and Nanotribology*, Springer Science & Business Media, Berlin, Germany **2001**.
[3] S. N. Gorb, *Proc. R. Soc. London, Ser. B* **1999**, *266*, 525.
[4] S. N. Gorb, P. P. Goodwyn, *J. Morphol.* **2003**, *257*, 127.
[5] D. S. Petersen, N. Kreuter, L. Heepe, S. Büsse, A. H. Wellbrock, K. Witte, S. N. Gorb, *J. Exp. Biol.* **2018**, *221*, jeb179242.
[6] S. N. Gorb, *Am. Entomol.* **2005**, *51*, 31.
[7] Y. Song, Z. Dai, Z. Wang, A. Ji, S. N. Gorb, *Sci. Rep.* **2016**, *6*, 26219.
[8] F. Haas, S. N. Gorb, *Arthropod Struct. Dev.* **2004**, *33*, 45.
[9] H. Marvi, D. L. Hu, *J. R. Soc. Interface* **2012**, *9*, 3067.
[10] H. T. Tramsen, S. N. Gorb, H. Zhang, P. Manoonpong, Z. Dai, L. Heepe, *J. R. Soc. Interface* **2018**, *15*, 20170629.
[11] J. Hazel, M. Stone, M. S. Grace, V. V. Tsukruk, *J. Biomech.* **1999**, *32*, 477.
[12] M. J. Baum, A. E. Kovalev, J. Michels, S. N. Gorb, *Tribol. Lett.* **2014**, *54*, 139.
[13] O. Unver, A. Uneri, A. Aydemir, M. Sitti, in *Proc. 2006 IEEE Int. Conf. on Robotics and Automation*, IEEE, Piscataway **2006**, p. 2329.
[14] K. A. Daltorio, A. D. Horchler, S. N. Gorb, R. E. Ritzmann, R. D. Quinn, in *2005 IEEE/RSJ Int. Conf. on Intelligent Robots and Systems*, IEEE, Piscataway **2005**, p. 4018.
[15] A. T. Asbeck, S. Kim, M. R. Cutkosky, W. R. Provancher, M. Lanzetta, *Int. J. Robot. Res* **2006**, *25*, 1165.
[16] M. J. Spenko, G. C. Haynes, J. A. Saunders, M. R. Cutkosky, A. A. Rizzi, R. J. Full, D. E. Koditschek, *J. Field Robot.* **2008**, *25*, 223.
[17] B. N. Persson, *J. Chem. Phys.* **2001**, *115*, 3840.
[18] E. Brown, N. Rodenberg, J. Amend, A. Mozeika, E. Steltz, M. R. Zakin, H. Lipson, H. M. Jaeger, *Proc. Natl. Acad. Sci. USA* **2010**, *107*, 18809.
[19] H. M. Jaeger, S. R. Nagel, R. P. Behringer, *Rev. Mod. Phys* **1996**, *68*, 1259.
[20] B. N. Persson, *Tribol. Lett.* **2016**, *62*, 34.
[21] V. L. Popov, *Contact Mechanics and Friction*, Springer, Berlin, Germany **2010**.
[22] H. M. Jaeger, *Soft Matter* **2015**, *11*, 12.
[23] T. S. Majmudar, M. Sperl, S. Luding, R. P. Behringer, *Phys. Rev. Lett* **2007**, *98*, 058001.
[24] M. E. Cates, J. P. Wittmer, J. P. Bouchaud, P. Claudin, *Phys. Rev. Lett* **1998**, *81*, 1841.
[25] B. Miller, C. O'Hern, R. P. Behringer, *Phys. Rev. Lett* **1996**, *77*, 3110.
[26] I. Albert, J. G. Sample, A. J. Morss, S. Rajagopalan, A. L. Barabási, P. Schiffer, *Phys. Rev. E* **2001**, *64*, 061303.
[27] Y. Forterre, O. Pouliquen, *Annu. Rev. Fluid Mech.* **2008**, *40*, 1.
[28] D. Bi, J. Zhang, B. Chakraborty, R. P. Behringer, *Nature* **2011**, *480*, 355.
[29] E. I. Corwin, H. M. Jaeger, S. R. Nagel, *Nature* **2005**, *435*, 1075.
[30] A. Tiwari, L. Dorogin, M. Tahir, K. W. Stöckelhuber, G. Heinrich, N. Espallargas, B. N. Persson, *Soft Matter* **2017**, *13*, 9103.
[31] N. K. Myshkin, M. I. Petrokovets, A. V. Kovalev, *Tribol. Int.* **2005**, *38*, 910.
[32] A. Jiang, T. Ranzani, G. Gerboni, L. Lekstutyte, K. Althoefer, P. Dasgupta, T. Nanayakkara, *Soft Robot.* **2014**, *1*, 192.
[33] N. G. Cheng, M. B. Lobovsky, S. J. Keating, A. M. Setapen, K. I. Gero, A. E. Hosoi, K. D. Iagnemma, in *2012 IEEE Int. Conf. on Robotics and Automation*, IEEE, Piscataway **2012**, p. 4328.
[34] A. J. Liu, S. R. Nagel, *Nature* **1998**, *396*, 21.
[35] A. Najmuddin, Y. Fukuoka, S. Ochiai, in *2012 IEEE/SICE Int. Symp. on System Integration (SII)*, IEEE, Piscataway **2012**, p. 248.
[36] R. Heise, V. L. Popov, *Tribol. Lett.* **2010**, *39*, 247.
[37] S. Hauser, K. Melo, M. Mutlu, A. Ijspeert, presented at *8th Int. Symp. on Adaptive Motion of Animals and Machines*, Sapporo, Japan, June **2017**.
[38] S. Hauser, M. Mutlu, P. Banzet, A. J. Ijspeert, *Adv. Rob.* **2018**, *32*, 825.

**ADVANCED
SCIENCE NEWS**

www.advancedsciencenews.com

**ADVANCED
MATERIALS
INTERFACES**

www.advmatinterfaces.de

[39] W. Thielicke, E. Stamhuis, *J. Open Res. Softw.* **2014**, *2*.

[40] W. Thielicke, *Ph.D. thesis*, University of Groningen **2014**.

[41] A. G. Athanassiadis, M. Z. Miskin, P. Kaplan, N. Rodenberg, S. H. Lee, J. Merritt, E. Brown, J. Amend, H. Lipson, H. M. Jaeger, *Soft Matter* **2014**, *10*, 48.

[42] M. Varenberg, S. N. Gorb, *Adv. Mater.* **2009**, *21*, 483.

[43] J. R. Amend, E. Brown, N. Rodenberg, H. M. Jaeger, H. Lipson, *IEEE Trans. Rob.* **2012**, *28*, 341.

[44] S. Hauser, P. Eckert, A. Tuleu, A. Ijspeert, in *2016 6th IEEE Int. Conf. on Biomedical Robotics and Biomechatronics (BioRob)*, IEEE, Piscataway **2016**, p. 1160.

[45] K. Hirai, M. Hirose, Y. Haikawa, T. Takenaka, in *Proc. 1998 IEEE Int. Conf. on Robotics and Automation (Cat. No. 98CH36146)*, Vol. *2*, IEEE, Piscataway **1998**, p. 1321.

[46] M. Raibert, K. Blankespoor, G. Nelson, R. Playter, *IFAC Proc. Vol.* **2008**, *41*, 10822.